In-Duct and Far-field Experimental Measurements from the ANCF for the Purpose of Improved Broadband Liner Optimization

Daniel L. Sutliff*
NASA Glenn Research Center
21000 Brookpark Road, Cleveland, OH 44135

Michael G. Jones† and Douglas M Nark‡
NASA Langley Research Center, Hampton
Hampton, VA 23681

A process for the design and evaluation of novel broadband acoustic liner concepts with limited fan source information is being evaluated. A pair of advanced broad-bandwidth liners were designed and manufactured for the NASA Glenn Research Center's Advanced Noise Control Fan (ANCF): (i) a constant impedance liner and (ii) a variable impedance liner. The insertion loss of both liners was measured in-duct utilizing the ANCF's Configurable Fan Artificial Noise System in a clean configuration with no-flow. Additionally, the acoustic characteristics of the Variable Impedance Liner were measured in the standard ANCF configuration with and without flow. The experimental setup, in-duct mode power levels, and far-field directivity are presented herein.

I. Introduction

As modern turbofan engines[1] incorporate increased bypass ratios and advanced fan designs, the broadband component of fan noise has grown in relevance. Therefore, while attenuation of fan tones remains a major consideration in engine nacelle acoustic liner design, the ability to simultaneously reduce broadband fan noise levels has become more important. A process for the design and evaluation of novel broadband acoustic liner concepts when limited fan source information is available was established in a previous study[2,3]. Specifically, a statistical fan source model was used within an acoustic duct propagation code to predict optimum impedance spectra for a benchmark scale model fan. Acoustic liner modeling tools were then used to identify geometric liner parameters (within manufacturing constraints) necessary to produce the impedance spectra that most closely matched the predicted optimum values. The resultant impedance values were then used with the propagation code to predict attenuation spectra and liner performance.

Two broadband liner designs were produced that were predicted to provide increased attenuation over conventional tonal designs for the full range of frequencies and operating conditions considered. Both designs incorporated a septum to create two-chambers. The 1st liner incorporated a septum with a constant depth to provide a constant impedance liner design (CIL). The 2nd design incorporated a unique variable depth septum creating a variable impedance liner (VIL). The insertion loss for each liner was measured experimentally on a low-speed fan. The objective of the experimental portion of this effort was to validate the efficacy of the design process by comparing the experimentally measured insertion losses for each liner to those predicted. The former is presented in this paper, and the latter in the companion paper[4].

*Aerospace Engineer, Acoustics Branch, MS 54-3, AIAA Associate Fellow
†Senior Research Scientist, Structural Acoustics Branch, MS 463, AIAA Associate Fellow
‡Senior Research Scientist, Acoustics Branch, MS 463, AIAA Associate Fellow

II. Experimental Setup

A. General Setup

The acoustic database to determine the efficacy of the design process was generated on the NASA Glenn Research Center's Advanced Noise Control Fan[5] (ANCF). The ANCF is a highly configurable 4-foot diameter ducted fan located in the Aero-Acoustic Propulsion Laboratory[6] (AAPL) at the NASA Glenn Research Center. The AAPL is a hemispherical anechoic (above 125 Hz.) test facility used for aero-acoustic research. An exterior view of the 65-foot high dome is shown in figure 1. The ANCF, shown in figure 2, operates inside a semi-enclosed, compact, far-field arena[7] such that it is in an anechoic environment. This allows for the continual acquisition of far-field data without moving the rig, or impacting the overall productivity of the other AAPL test rigs.

The Configurable Fan Artificial Noise System[8] (CFANS) was utilized to generate and control circumferential modes. The system consists of 4 axially distributed rows, each with 16 circumferentially distributed sets of electromagnetic drivers flush mounted on the inner wall. The practical limits of the system are $|\text{m-order}| \leq 7$, and frequency ≤ 1500 Hz for mode generation. The modes were measured by the Rotating Rake mode measurement system. The Rotating Rake[9] system was developed and implemented by the NASA Glenn Research Center in the 1990s to measure turbofan acoustic duct modes. The system is a continuously rotating radial microphone rake that is inserted into the duct. It provides a complete map of the acoustic duct modes present in a ducted fan.

Table I provides the individual circumferential modes generated and the corresponding radial modes cut-on for two hub-to-tip ratios (σ) inside the duct, for the studies documented in this paper. The maximum circumferential mode (m) that could be cut-on is presented also. For each frequency, the m-orders (0,…,6) were generated individually. The characteristics of single mode generation were presented in reference 8. In addition, a table with randomized phases was created to generate all modes, in a repeatable fashion. Examples of the modal signatures generated in this fashion are shown in figure 3. The left side of the figure presents results with the rake position near the duct exit for two different builds (fig 3a,b) and the difference between the two (fig 3c). The right side of the figure shows the modal structure at a position near mid-duct for two different builds (fig 3d,e) and the difference (fig 3f). The total PWL difference is with-in 1 dB, and the individual modes generally vary about +/- 1 dB, with a few outliers with as high as a 4 dB difference.

In addition, the CFANS was modified to provide a broadband signal. A signal generator out-putting a 500-5000 Hz bandwidth white noise signal to all drivers was utilized. No attempt was made to compensate for driver response or to generate a modal structure.

B. Vertical Orientation

In order to provide a clean, annular duct for this experiment the ANCF was built up off of the stanchion/pylon assembly that normally supports the fan and duct sections that make up the nacelle. That is, the spool pieces were stacked up in a vertical orientation on the floor. This removed center-body and support pylon from the arrangement, providing a constant area annular duct. Two configurations were tested in this setup: (i) with a constant 24" diameter cylindrical tube and (ii) with a constant 36" diameter cylindrical tube. (Figure 4.) These provided an equivalent annular duct hub-to-tip ratio of 0.5 and 0.75, respectively. The entire stack rested on the floor, and approximately 6" of foam material was placed in the bottom of the stack to minimize reflections from the floor. Only in-duct rotating rake measurements using the CFANS as a source were acquired in this configuration. Obviously, in this orientation, there was no flow. Rotating Rake data were acquired at the entrance, and exit of the liner. This was the primary setup for all liner configurations.

C. Horizontal Orientation

Selected liner configurations were also installed on the standard ANCF configuration (see figure 5). The fan was used as the primary source at the standard range of 1400-2000 rpm. Two stator counts were utilized, 0 (rotor alone) and 14 vanes at 0.5 chord spacing. The liner was installed in the aft converging section where the hub-to-tip ratio transitions from 0.375 to 0.5. Rotating rake measurements upstream, and downstream of the liner were acquired. Far-field directivity measurements were acquired. The CFANS was used to generate broadband noise as described above (no flow) and far-field measurements acquired.

Figure 1. Aero-Acoustic Propulsion Laboratory.

Figure 2. Advanced Noise Control Fan.

TABLE I: Modes Generated for Parametric Studies using CFANS

		HIGHEST MODES CUT-ON	
FREQ (Hz)	CIRCUM MODE GENERATED	σ=0.50 n_{max} (m_{max})	σ=.75 n_{max} (m_{max})
500	0,1,2,3,4,5,6,R	0,0,0,0,0,0,0 (4)	0,0,0,0,0,0,0 (4)
700	0,1,2,3,4,5,6,R	1,1,1,1,0,0,0 (6)	1,1,1,1,0,0,0 (6)
900	0,1,2,3,4,5,6,R	1,1,1,1,1,1,0 (8)	1,1,1,1,1,1,0 (8)
1100	0,1,2,3,4,5,6,R	1,1,1,1,1,1,1 (10)	1,1,1,1,1,1,1 (11)
1300	0,1,2,3,4,5,6,R	2,2,2,2,2,2,1 (12)	2,2,2,2,2,2,1 (13)
1500	0,1,2,3,4,5,6,R	2,2,2,2,2,2,2 (14)	2,2,2,2,2,2,2 (15)

Note: R = random modes, *n*=radial mode, *m* = circumferential mode, σ = hub-to-tip ratio

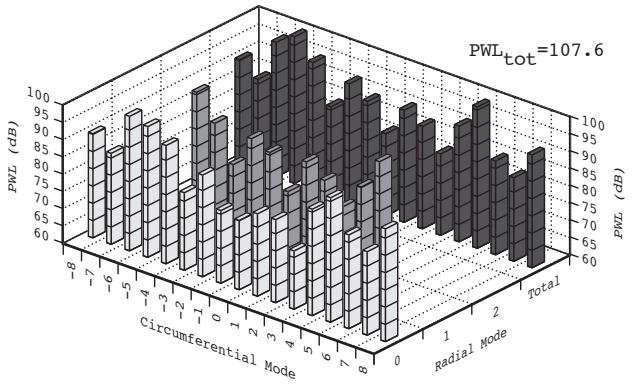

a) Rake Position Near Duct Exit (Build 1)

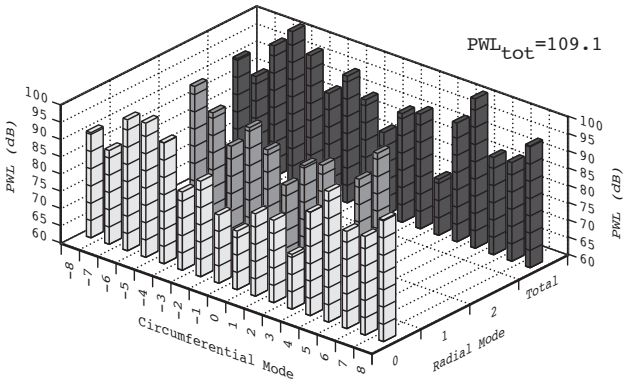

d) Rake Position Near Mid-Duct (Build 1)

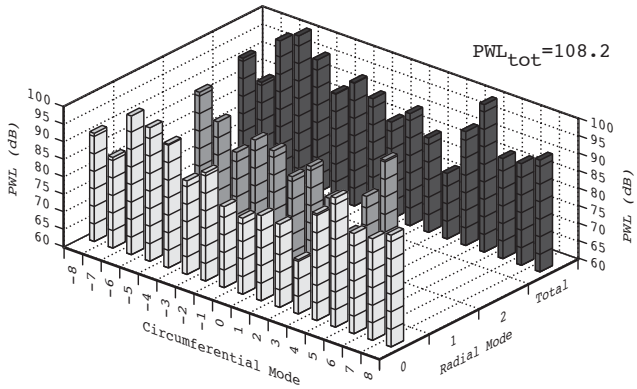

b) Rake Position Near Duct Exit (Build 2)

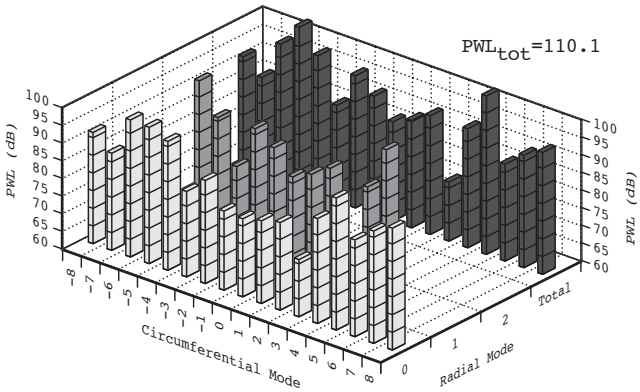

e) Rake Position Near Mid-Duct (Build 2)

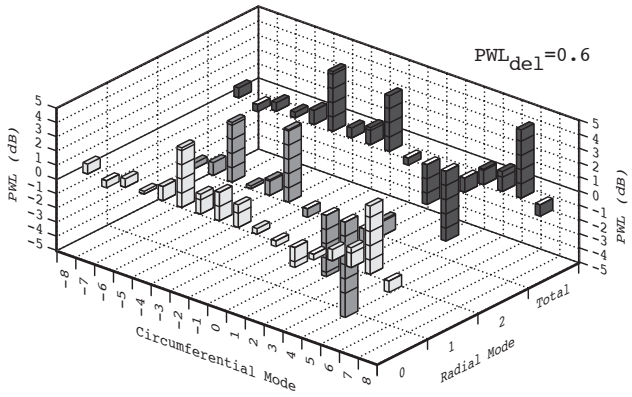

c) Rake Position Near Duct Exit (delta-PWL)

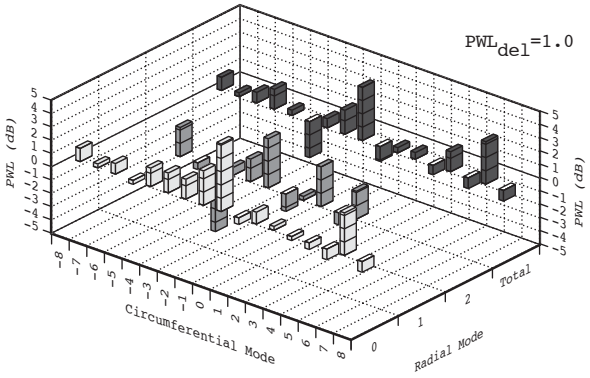

f) Rake Position Near Mid-Duct (delta-PWL)

Figure 3. Random Mode Generation Power Level Distribution in Hard-wall Configuration. Random modes excited @ 900 Hz with 24” Center-body in Vertical Orientation.

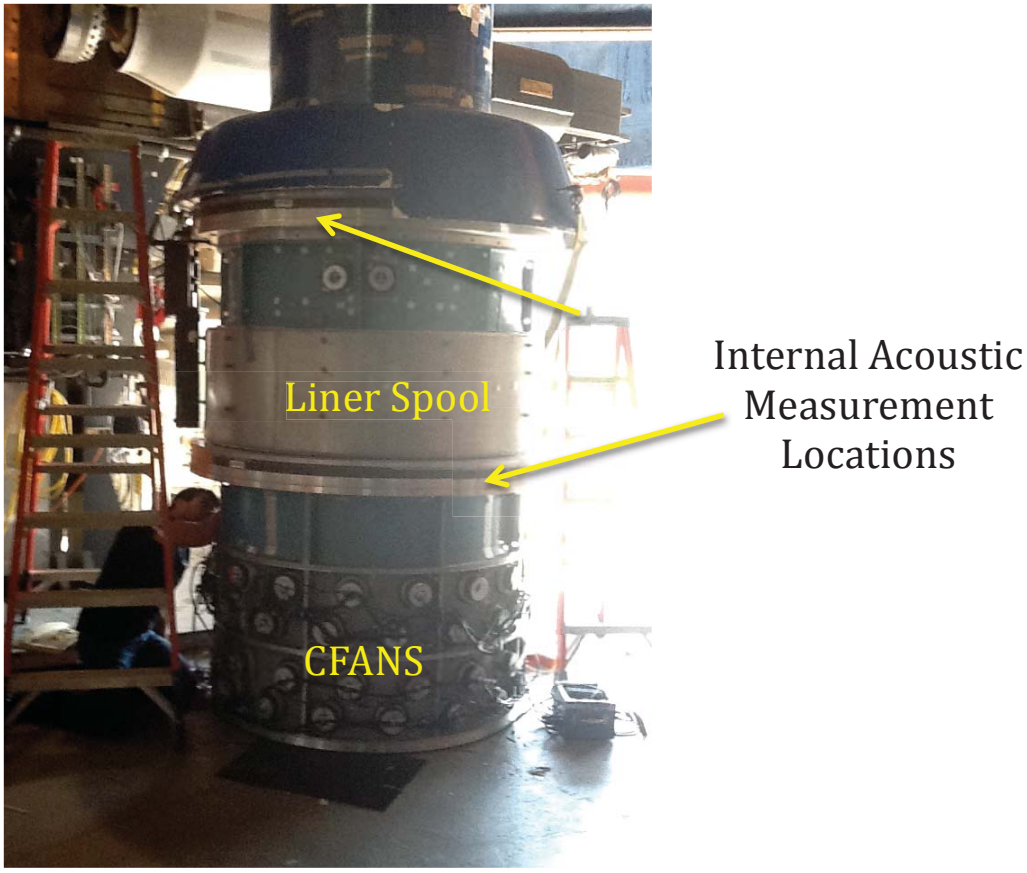

Figure 4. Stack-up in Vertical, Off-Stanchion Orientation. (No Flow).

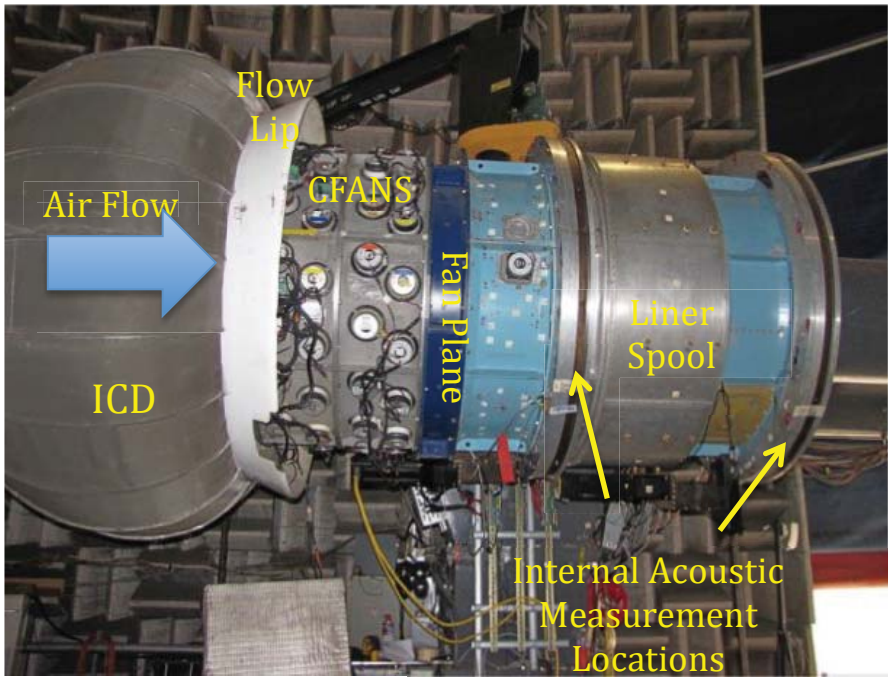

Figure 5. Build-up in Horizontal, Standard, On-Stanchion Orientation (Flow & No-Flow).

D. Assembly of liners for ANCF

Two liner cores were designed and manufactured for this test program, a Constant Impedance Liner and a Variable Impedance Liner. Described in this section is the assembly of the core into a spool for installation on the ANCF. The effective axial length of the liner core was 16 inches and was on the outer wall of the 48" spool piece. The design process, acoustic specifications, and predicted performance of the liner cores are detailed in reference 4.

The liner cores were manufactured separately and individually incorporated into an existing spool piece. Starting from the outer radius working inward, the liner assembly was as follows (see figure 6). First, 2 layers of carpet padding were laid in the spool in order to provide a compression mechanism for the entire assembly. This mitigated the geometric imperfections of the spool wall, ultimately allowing for a tight fit. Next, a hard rubber sheet was laid down. This provided a seal at the base of the honeycomb core to prevent acoustic leakage between the cells. On top of this was placed one of the two cores. Both cores had a total thickness of 2.0 inches. For the CIL core, an 800 MKS Rayls septum was embedded in each cell at a constant penetration height (h_1 in figure xxx) of 1.25 inches. The VIL core was comprised of repeated groups of four cells. Two of these cells had a septum penetration height of 1.25 inches, with DC flow resistances of 1100 and 1200 MKS Rayls, respectively. The other two cells had a penetration height of 1.30 inches and a septum flow resistance of 1100 MKS Rayls.A fine wire mesh (DC flow resistance of 20 MKS Rayls) was placed on top of the core, followed by a coarse screen covering (~25% open area). This screen was fastened to the facing of the inner ledge of the spool frame in such a manner to compress the entire lay-up securely and provide a flush flow surface in the duct. Photographs of a liner assembly sample are shown in figure 7. The septum is seen in figure 7b. Figure 8 shows the liner assembly installed in the ANCF spool.

The CIL and VIL cores were tested in separate assemblies. The primary configurations were the liner fully exposed and fully covered with aluminum tape to mimic a hard-wall condition. Portioning sections of the liner and covering them with the Al-tape created secondary configurations. This provided a larger database and the opportunity to study the efficacy of the prediction methodology on segmented liners. Figure 9 provides a visual representation of the 5 liner plan-forms "un-rolled" for the various segmented liners. The key dimensions are shown in Table II (assume the leading edge of the liner is at x=0").

The CIL and VIL were both tested in the vertical orientation (no flow) with the 24" center-body. All 5 liner plan-forms were tested. Only the VIL was tested in the 36" center-body vertical configuration (also for all 5 plan-forms). The full set of frequencies from Table I were generated, Rotating Rake data were acquired at the entrance and exit of the installed liner, for the primary liner plan-forms (hard-wall, and fully exposed) and a reduced set of frequencies for the segmented liner plan-forms.

The VIL primary liner plan-forms were tested on the ANCF on-stanchion. Rotating Rake data were acquired at the upstream and downstream of the installed liner with the fan as a source with 0 (rotor alone) or 14 vanes over the standard RPM range. Far-field directivity data were also acquired for these configurations. In addition, the CFANS was modified to provide a broadband signal (from prior experience the fan is run at idle to provide a consistent blockage between configurations–essentially no flow). Far-field directivity data were acquired for the hard-wall and fully exposed liner plan-forms.

The types of data acquired are shown on Table III for each orientation, configuration, and plan-form tested.

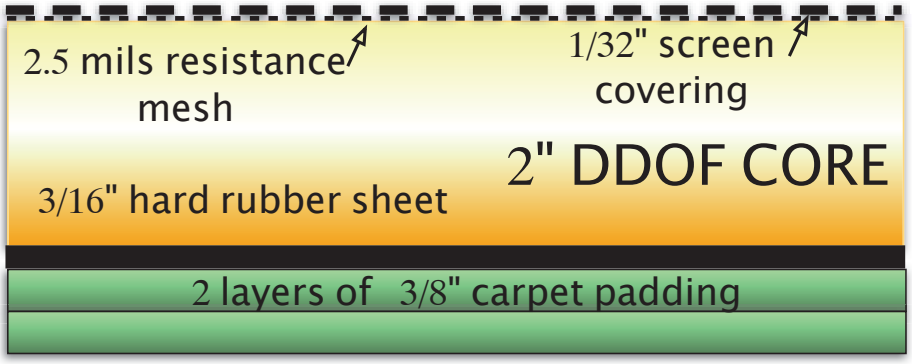

Figure 6. Cross-Section Schematic of Liner Assembly.

(a) Top View

(b) Side View

Figure 7. Liner Build-up Photographs.

(a) Existing Spool Showing Empty Pocket.

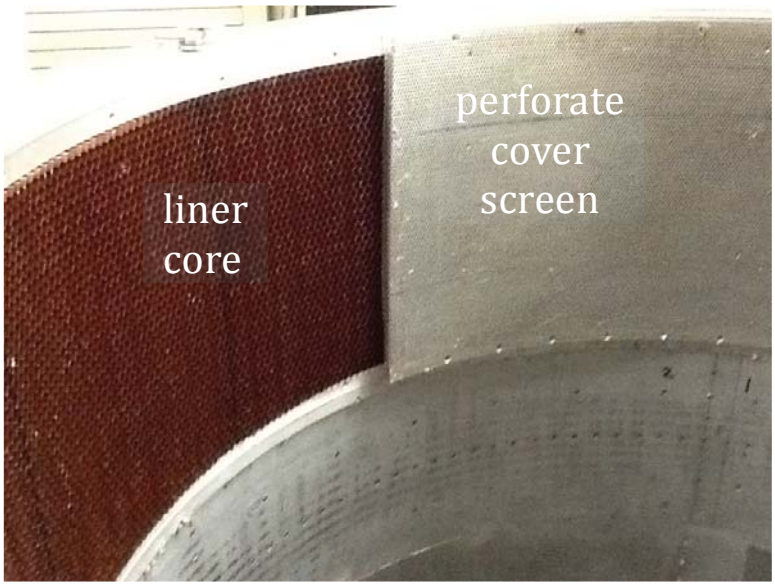

(b) Top View

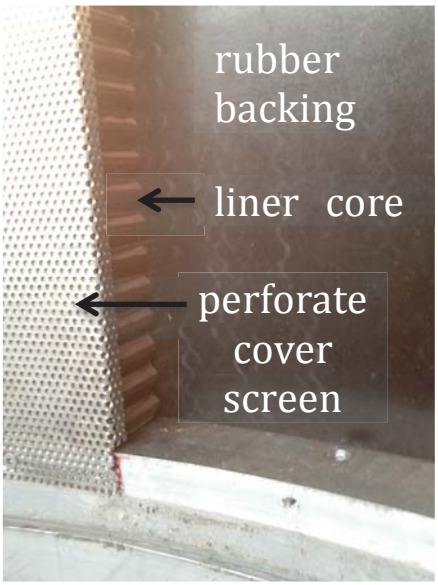

(c) Side View

Figure 8. Liner Spool Build-up Photographs.

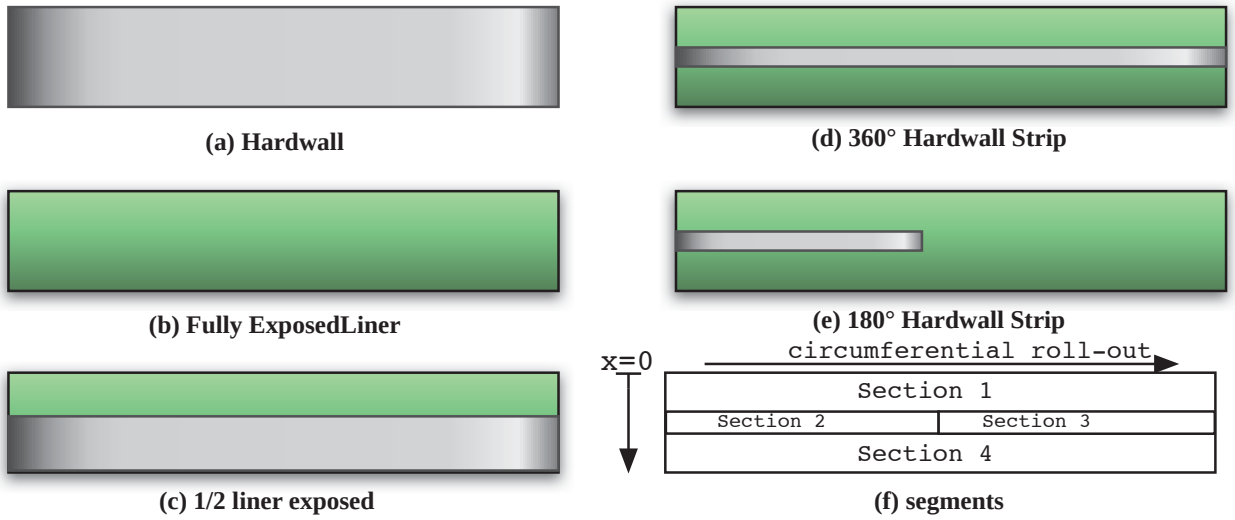

Figure 9. Liner Configurations Tested.

TABLE II: Dimensions of Liner Configurations

	Axial LE (in)	Axial TE (in)	Arc
Section 1	0	7	$0 < \theta < 360°$
Section 2	7	9	$0 < \theta < 180°$
Section 3	7	9	$180 < \theta < 360°$
Section 4	9	16	$0 < \theta < 360°$

TABLE III: Test Matrix

Configuration	Liner	Segments (see fig 9)	Data Acquired	Source	Signal
CB24	CIL	a,b	RRx2	CFANS	700,900,1100,1300,1500 Hz; R
""	""	c,d,e	"	""	700,1100,1500 Hz; R
CB24	VIL	a,b	RRx2	CFANS	700,900,1100,1300,1500 Hz; R
""	""	c,d,e	"	""	700,1100,1500 Hz; R
CB36	VIL	a,b	RRx2	CFANS	700,900,1100,1300,1500 Hz; R
""	""	c,d,e	"	""	700,1100,1500 Hz; R
ANCF	VIL	a,b	FF	CFANS	Broadband
ANCF–Fan(0,14V)	VIL	a,b	RRx2, FF	Fan	1400,1600,1800,2000 rpm

CB24 : 24" diameter center body, CB36 : 36" diameter center body; ANCF = on stanchion
CIL : constant impedance liner; VIL : variable impedance liner
RRx2 : Rotating Rake at 2 locations, FF : Far-field

III. Results

A limited selection of the results is presented in this section. For details of how the data were acquired and processed see reference 10. Keep in mind that the liners were not individually designed for optimum attenuation, but rather to validate the design and manufacture process. Compare the results to the predictions in reference 4.

A. In-Duct

Samples of the modal decomposition from the rotating rake are shown in figure 10. These cases are with the CFANS generating random modes at 900 Hz for the hard wall and fully exposed liner plan-forms. The radial and circumferential mode power, total power in the tone is presented, and the insertion loss is computed.

The left column (figs 10a,b,c) presents the modal decompositions with the Constant Impedance Liner (CIL) installed with a 24" center-body. The center column (figs 10d,e,f) present the modal decomposition with the Variable Impedance Liner (VIL) installed with a 24" center-body. The right column (figs 10g,h,i) present the modal decomposition with the Variable Impedance Liner (VIL) installed with a 36" center-body. In each case the top row is data acquired with the rotating rake installed at the exit of the liner, the middle row rake is data from the exit of the liner, and the bottom row the insertion loss for that configuration. The CIL and VIL (24" CB) perform similarly with insertion losses of 6.0 and 7.5 dB PWL, respectively. The individual mode attenuation is greater at the higher circumferential modes, most likely due to higher wave number as the cut-off ratio approaches 1. Significant additional insertion loss (12.8 dB PWL) is obtained from the VIL installed in the 36" center-body configuration. Also the influence of cut-off ratio is less pronounced, with noticeable attenuation occurring even at lower m-order, highly cut-on modes.

The insertion loss was computed for the three vertical and the horizontal (standard ANCF) configurations for the remaining frequencies and plotted on figure 11. The solid lines show the insertion losses for the 3 liner configurations. The CIL and VIL perform reasonably similar across the frequency range, as they were designed (see reference 4. When the VIL is coupled with the 36" center-body the insertion loss is greater, which also was predicted by the design methodology. The dashed lines indicate the insertion loss for the hard-wall baseline for both center-bodies. A slight loss (~2 dB) is measured. This is a little outside the uncertainty, (~1 dB) and may be due to a reflection from the duct exit or the termination at the floor. Other attenuation factors in the set-up (e.g. it is assumed that the cardboard tube comprising the center-body provides a hard-wall boundary condition and does not introduce any structural-acoustic coupling) may be present. A repeat case occurs when comparing the hard-wall values obtained in the hard-wall baselines for the CIL and VIL each installed with the 24" center-body (achieved by taping over each of the liners) and is remarkably consistent. Added to this plot are data from the VIL installed on the ANCF with the rotor alone as a source. More points are plotted here because the 1st three harmonics of the blade passing frequency (BPF) are plotted for each fan rpm. The breaks in the lines indicate the jump to a higher harmonic. Note that the ANCF center-body does vary from the rotor plane to the constant area section at exit, The constant area section has a 24" center-body, and about 75% of the liner is in this section; the leading 25% is in the converging section. This would clearly affect the liner performance.

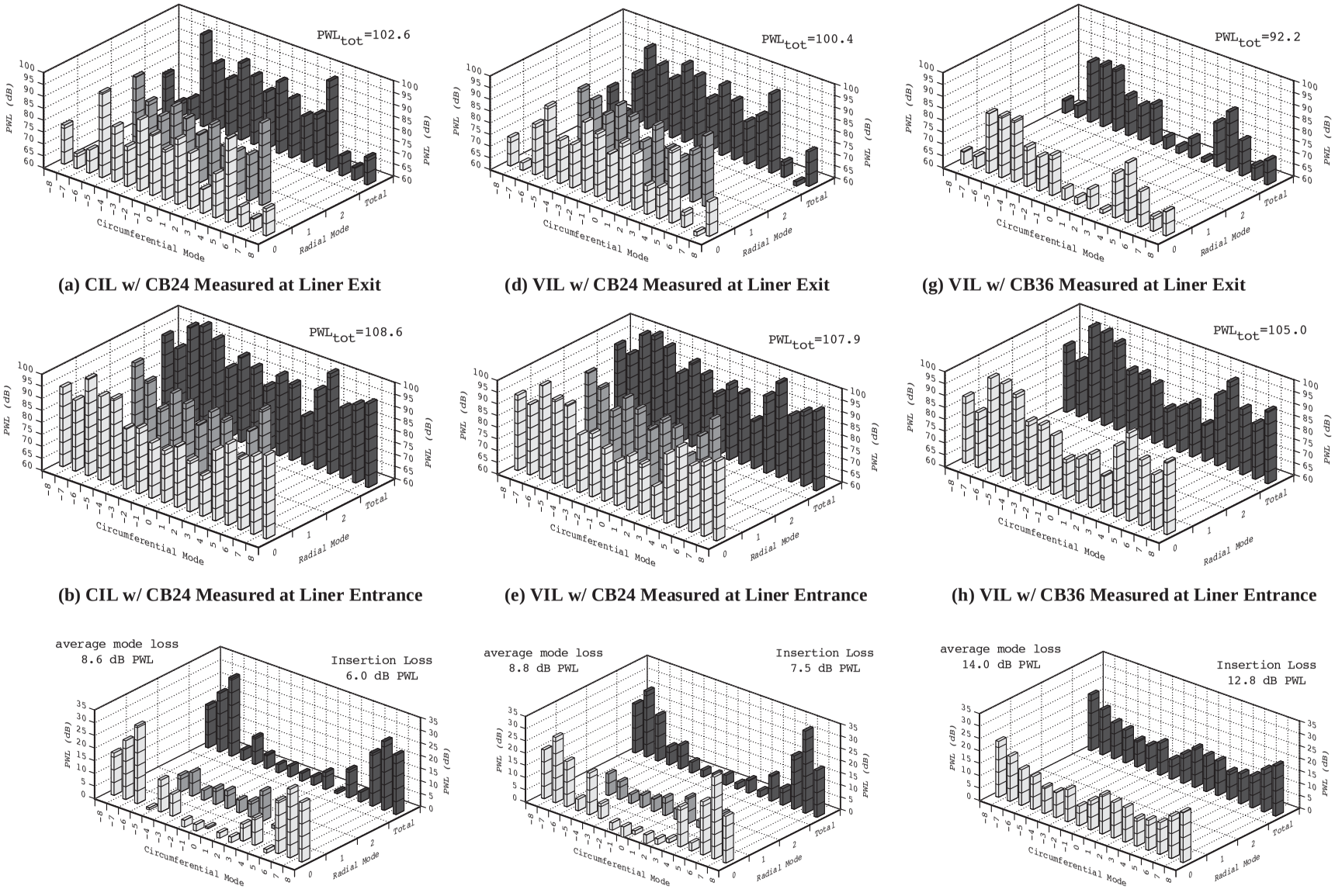

(a) CIL w/ CB24 Measured at Liner Exit

(d) VIL w/ CB24 Measured at Liner Exit

(g) VIL w/ CB36 Measured at Liner Exit

(b) CIL w/ CB24 Measured at Liner Entrance

(e) VIL w/ CB24 Measured at Liner Entrance

(h) VIL w/ CB36 Measured at Liner Entrance

(c) CIL w/ CB24 Insertion Loss

(f) VIL w/ CB24 Insertion Loss

(i) VIL w/ CB36 Insertion Loss

Figure 10. Mode Power Level Distribution and Insertion Losses. Random Modes Excited @ 900 Hz.

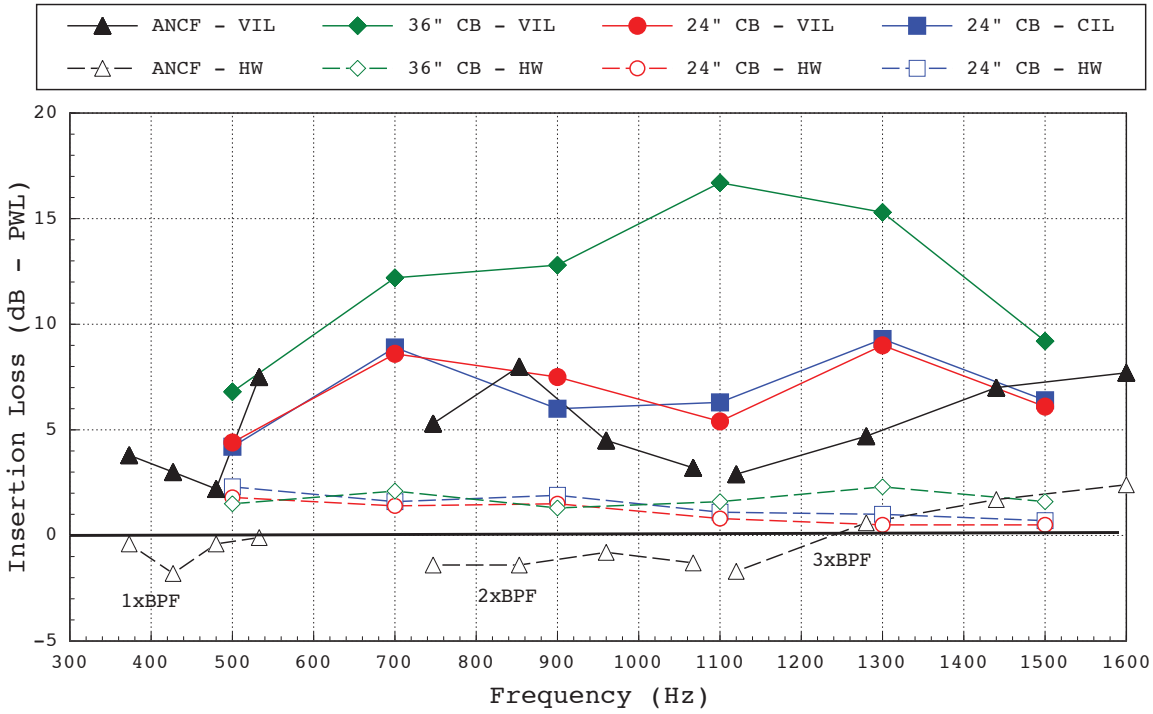

Figure 11. Insertion Loss vs Frequency for Multiple Configurations.

B. Far-field

Samples of the directivity of the attenuation of the far-field broadband component are presented in figure 12 for the VIL installed on the ANCF in the standard horizontal, on-stanchion build-up. Figure 12a is obtained with the CFANS generating a signal from an input of white noise with a bandwidth of 500 – 5000 Hz. In this case the flow is essentially zero, though the fan is at idle. The plot shows the computed PWL at each angle for the fully exposed liner subtracted from the hard-wall case (positive number is an attenuation) separated out by the harmonic bands. There is little or no change in the PWL in the forward sector (0°-180°) as there is no treatment in the inlet. The attenuation peaks in the aft sector at the 1750 – 2250 Hz band (4th harmonic band). Figure 12b shows the same computation except the source was the fan running at 2000 rpm. The attenuation is lower when the fan is the source. This could be a Mach number effect, though it is relatively low (< 0.2). Alternatively the floor could be set by external noise sources (flow over the aft pylon, jet noise, etc.).

Figure 13 shows the same data integrated over the harmonic bands with the forward and aft arcs separated. A slight reflection is noted in the forward arc for the CFANS case. The change at the 1st harmonic band with the fan as a source is probably due to the more variable levels at low (below BPF) resulting from sensitivity to turbulence.

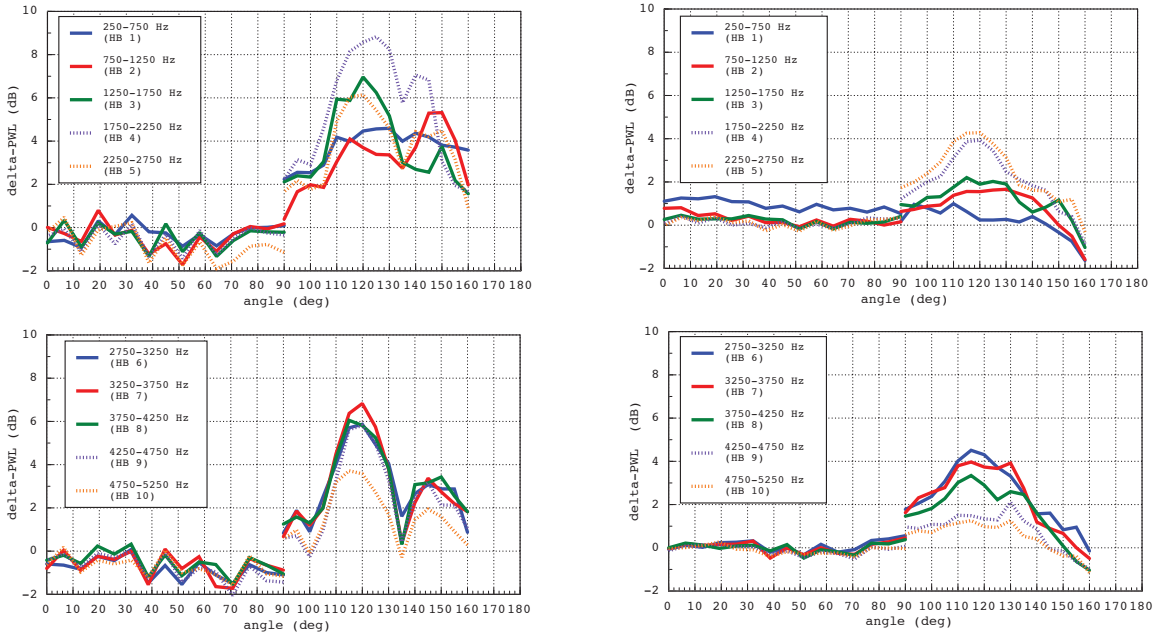

(a) CFANS Generating White Noise (no-flow) **(b) Fan @ 2000 rpm – rotor alone (flow)**

Figure 12. Attenuated Far-field Power Levels. Variable Impedance Liner Installed on ANCF. Lip Installed on Duct Exit Flange. Harmonics Centered on 2000 rpm (533 Hz) Equivalent BPF.

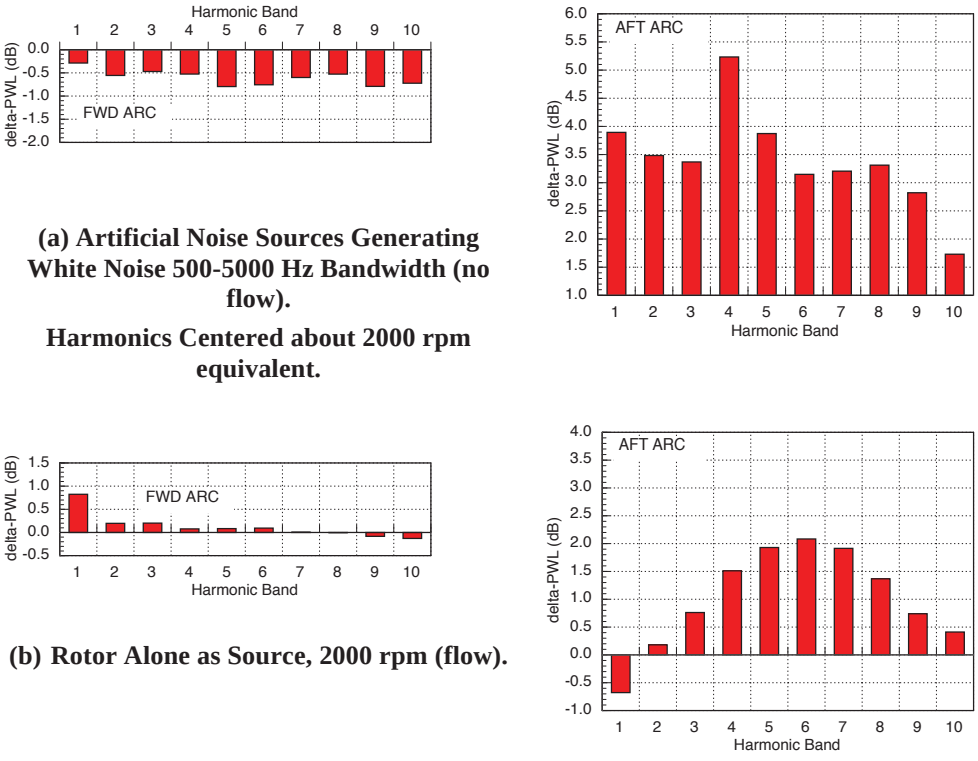

(a) Artificial Noise Sources Generating White Noise 500-5000 Hz Bandwidth (no flow).

Harmonics Centered about 2000 rpm equivalent.

(b) Rotor Alone as Source, 2000 rpm (flow).

Figure 13. Attenuated Far-field Power Levels Integrated over Harmonic Band. Variable Impedance Liner Installed on ANCF. Lip Installed on Duct Exit Flange.

C. Comparisons to Numerical Prediction

Selected insertion loss predictions from reference 4 are compared with the experimentally measured in Figure 14. The predictions are a mean of multiple runs of random amplitudes and phases, while the experimental measurements are from a single set of random modes (which were created by sending a unity amplitude signal with a random phase to each driver), repeated. The 95% confidence distribution bar for the predictions is placed on the right side of the graphs. From experience the measurement error is +/- 1 dB. Other measurement errors can arise due to duct reflections[11,12].

Figure 14a shows the insertion loss vs. frequency for the CIL. Most of the points could be considered within the uncertainty range or just outside. Figure 14b shows the comparison for the VIL. For the 24" center-body the comparisons are similar, within the uncertainty range or just outside. The difference between the predictions and measurements for the 36" VIL center body is more generally outside the uncertainty, but the trend of the curves match. In addition the increased performance of the VIL of the 36" center-body relative to the 24". The relative performance of the two liners with the 24" center-body (compare across sub-plots) compares well for the predictions and measurements.

The generally higher measured insertion loss compared to the predicted may be a consequence of duct reflections affecting the experimental results, perhaps due to the center-body boundary conditions. Another possibility may be the physical difference between running a single, phase-randomized, but fixed, distribution of modes compared to a fully random set of many modal distributions.

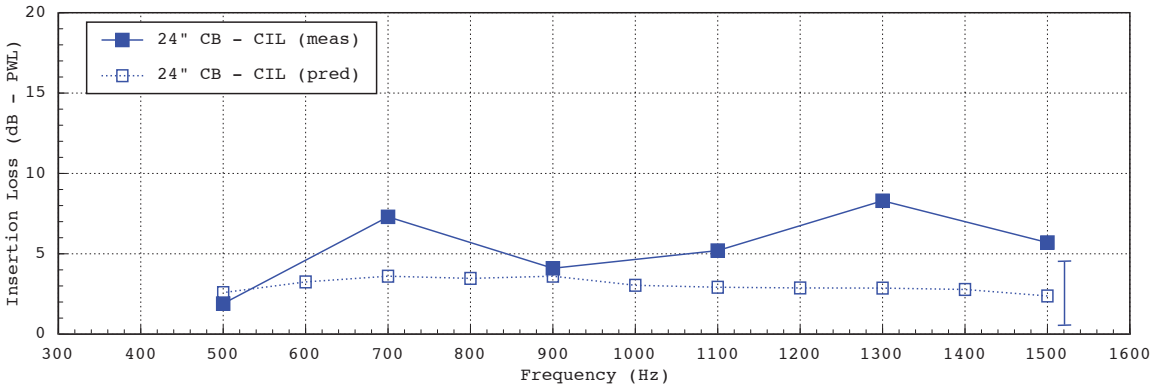

(a) Constant Impedance Liner.

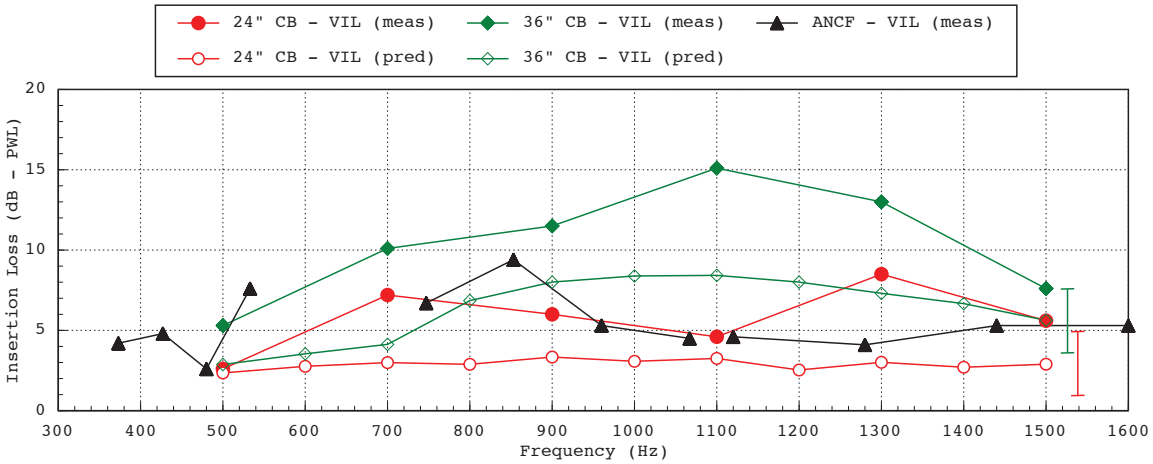

(b) Variable Impedance Liner.

Figure 14. Insertion Loss Comparison of Experimental Measurement to Numerical Prediction.

IV. Conclusion

Parametric sets of insertion loss databases were acquired for the purpose of validating a design and manufacturing methodology. A Constant Impedance Liner and Variable Impedance Liner were evaluated using the Glenn Research Center's Advanced Noise Control Fan (ANCF) operating the Configurable Fan Artificial Noise Source system in a novel, clean, vertical build. Each liner was installed coupled to two center-bodies (24" and 36"). A variety of liner plan-forms were evaluated. Insertion loss for each configuration was measured in-duct using the Rotating Rake measurement system, and far-field directivity was acquired with the VIL installed on the ANCF in the traditional build. The data were acquired in support of a companion paper that describes the design and prediction methodology (reference 4). Overall, the predicted and measurement trends agreed very well. In some cases the insertion losses were under predicted relative to the measurements. The geometry and data acquired from the CIL are available upon written request.

V. ACKNOWLEDGEMENTS

The authors world like to acknowledge the efforts of D. Podboy, L. Smith, R. Loew, B. Groening, E. Mysliwiec, and J. Mirecki of TFOME for their support in model assembly and testing. The contributions of Hexcel, Inc,. led by Clark Smith, Earl Ayle, and Fumitaka Ichihashi were key to the success of this effort.

This work was supported by the Fundamental Aeronautics Program / Fixed Wing Project.

VI. References

[1]H.H. Hubbard, editor, Aeroacoustics of Flight Vehicles: Theory and Practice: Volume 1, NASA Reference Publication 1258, Vol 1, WRDC Technical Report 90-3052.

[2]D.M. Nark, and M.G. Jones, "Broadband Liner Optimization for the Source Diagnostic Test Fan," AIAA Paper 2012-2195.

[3]D.M. Nark, F. Farassat, D.S. Pope, and V. Vatsa, "The Development of the Ducted Fan Noise Propagation and Radiation Code CDUCTLaRC", AIAA Paper 2003-3242.

[4]D.M. Nark, M.G. Jones, and D.L. Sutliff, "Improved Broadband Liner Optimization Applied to the Advanced Noise Control Fan", 2014 AIAA Aviation and Aeroacoustics Forum, Atalanta, Georgia (to be published).

[5]R.A. Loew, J.T. Lauer, J. MCAllister, and D.L. Sutliff, "The Advanced Noise Control Fan", NASA/TM–2006-214368, also AIAA–2006-3150, Nov 2006.

[6]B.A. Cooper, "A Large Hemi-Anechoic Chamber Enclosure for Community-Compatible Aeroacoustic Testing of Aircraft Propulsion Systems", Journal of the Institute of Noise Control Engineering of the USA, Jan/Feb 1994.

[7]D.L. Sutliff, "Acoustic Characteristics of the Active Noise Control Fan Located in the Compact Farfield Arena", Technical Progress Report, Contract NAS3-00170, Task Order no. 17, Sest Inc.

[8]D.L. Sutliff, "A Mode Propagation Database Suitable for Code Validation Utilizing the NASA Glenn Advanced Noise Control Fan and Artificial Sources", AIAA Paper 2014-0719.

[9]D.L. Sutliff. "Rotating Rake Turbofan Duct Mode Measurement System", International Journal of Aeroacoustics, June 2007.

[10]J. McAllister, R.A. Loew, J.T. Lauer, and D.L. Sutliff, "The Advanced Noise Control Fan Baseline Measurements", NASA/TM–2009-215595, also AIAA–2009-0624, Oct 2009.

[11] M.D. Dahl, et. al., "Assessment of NASA's Aircraft Noise Prediction Capability" , NASA/TP–2012-215653, July 2012.

[12] M.D. Dahl, D.R. Hixon, and D.L. Sutliff, "Further Development of Rotating Rake Mode Measurement Data Analysis ", AIAA 2013-2246"